ANALYSIS OF EXPERIMENTAL DATA ON THE HIGH-ENERGY END OF THE ^{252}CF SPONTANEOUS-FISSION NEUTRON SPECTRUM

H. Märten, D. Richter, and D. Seeliger

Technical University Dresden
8027 Dresden, Mommsenstraße 13
German Democratic Republic

Abstract

General characteristics of the analysis of experimental data on the high-energy end of fission neutron spectra are summarized and described in the case of the neutron energy distribution from spontaneous fission of ^{252}Cf.

The analysis procedures pertain to the two-dimensional measurement of neutron time-of-flight (TOF) and scintillator response (light output LO). Both the (TOF, LO)-spectroscopy and the efficient background suppression render it possible to measure very low emission probabilities N(E) which are typical at high emission energies E.

The report includes a specification of essential data corrections and the error estimation.

1. Introduction

As pointed out by Blinov in his review paper[1], experimental data on the high-energy tail of the $^{252}Cf(sf)$ neutron spectrum diverge strongly. This is due to the rather low emission probability of fission neutrons at high E.
In the case of the common TOF-spectroscopy at a fixed light output (LO) bias B, the foreground/background ratios are insufficient at high neutron energies. Such experiments cover the energy range up to about 15 MeV.

Therefore, we apply the two-dimensional (TOF, LO)-spectroscopy which enables the selection of the optimum LO bias as a function of neutron energy. In this way, the experimental errors are minimized. The corresponding analysis procedures as well as data corrections, which are essential for the neutron spectroscopy at high emission energies, are described in this report. It includes informations on the error evaluation also.

The precise measurement of the $^{252}Cf(sf)$ neutron spectrum at high energies is serviceable to fix a data evaluation at high E. A new evaluation was strongly recommended at the IAEA Consultants' Meeting[2]. Further, informations on the mechanism of fission neutron emission are expected[3-5].

Preliminary results of the $^{252}Cf(sf)$-N(E)-measurement were presented in Ref. 6, 7. The analysis of these data was somewhat refined concerning (i) the LO calibration, (ii) the detector efficiency determination, and (iii) the time resolution consideration. The energy range of the analysed neutron spectrum was extended to lower energies. The hitherto published data on the highest-energy end (E higher than 20 MeV) are unchanged. The final spectrum is compared with theoretical spectrum calculations[4], with the NBS evaluation[8] as well as recent experimental data as far as concerning the high-energy region[9-11].

2. The neutron (TOF,LO)-spectroscopy

Fig. 1 illustrates the two-dimensional (TOF-LO)-spectroscopy schematically. Fission neutrons are detected within a fixed solid angle $\Delta\Omega$ with an efficiency $\varepsilon(E,B)$. Some of the secondary effects like neutron scattering and absorption by detector walls, the collimator, and air are indicated partly. The neutron TOF is measured applying a time-to-amplitude converter (TAC) which analyses the time difference of the fast signals from both the fission fragment (FF) detector and the neutron detector. Commonly, the fragment detector signal is delayed by at least a time which is equal to the chosen TAC time range. It is used as the STOP signal to avoid dead-time losses, i.e. the time scale is inverted. In the present case, the LO signal is deduced from the neutron detector signal by integration (about 100 ns time constant).

The neutron detector is also sensitive to γ-rays and penetrating charged cosmic rays (myons with energies around 1 GeV especially[12]). Applying a NE 213 scintillator and using the charge-comparison method[13], such background events are suppressed efficiently except cosmic protons. Their intensity is reduced by a heavy shielding. The LO spectrum of cosmic rays depends on scintillator dimensions strongly. If using a voluminous scintillator as suitable for the spectroscopy of high-energy fission neutrons, the cosmic-particle events appear at rather high detector pulse heights predominantly (cp. Ref. 6, 7). The $n/\gamma/\mu$-discrimination method as well as the two-dimensional (TOF,LO)-measurement are the main prerequisites for the high-sensitive spectroscopy of fission neutrons at high E.

Fig. 2 represents a two-dimensional (TOF,LO)-spectrum consisting of the γ-line (γ-TOF peak) and the neutron event region which is limited according to kinematics of neutron-proton scattering. The scintillator response function for a given TOF channel, i.e. fixed E, extends to an edge which corresponds to the maximum proton recoil energy approximatively. Scattered neutrons give rise to events at rather high TOF, but comparatively high LO are possible.

The regions I and II indicated in Fig. 2 may be used for the determination of the random background. However, region I is suitable at sufficiently high LO only, because this spectrum field might be influenced by non-suppressed low-energy γ-rays which are emitted from fragments with excitation energies below the neutron separation energy within about 10^{-6} s after scission. In general, the γ-peak position weakly depends on LO in spite of developed timing methods (cp. Fig. 2a). A further TOF-channel-dependent background part appears due to accidental STOP events. It can be avoided by a pile-up rejector electronically[9] or considered analytically[10].

Fig. 2b shows a typical TOF distribution for a fixed LO bias and indicates its different constituents, i.e. the remaining γ-peak, the random as well as the TOF-channel-dependent background, the scattered-neutron distribution, and the real fission-neutron TOF spectrum to be analysed.

The time resolution with regard to the γ-peak Δt_γ is a function of LO generally. This dependence $\Delta t_\gamma(LO)$ (FWHM) can be determined by analysing the γ-peak for different LO channels from a measurement without n/γ/μ-discrimination. The whole neutron TOF resolution Δt_n is neutron-energy-dependent due to the scintillator thickness d and can be expressed by

$$\Delta t_n(E,LO) = \left[\Delta t_\gamma^3(LO) + \Delta t_{sc}^3(E) \right]^{1/3} \qquad (1)$$

(cp. Ref. 14 concerning the superposition of a Gaussian distribution with a rectangular distribution like the detection time distribution) where the time-of-flight of a neutron with the energy E for a distance d is

$$\Delta t_{sc}(E)/ns = 0.723 \cdot d/cm \cdot (E/MeV)^{-1/2}. \qquad (2)$$

Hence, the actual neutron TOF distribution n(t:LO) for a fixed LO (t - neutron TOF) is folded by the time resolution function $T(t,\tau:LO)$ which is assumed to be Gaussian, i.e.

$$T(t,\tau:LO) = (\sigma\cdot\sqrt{2\pi})^{-1} \cdot \exp(-(t-\tau)^2/(2\cdot\sigma^2)) \qquad (3)$$

where

$$\sigma = \sigma(t(E),LO) \approx 0.425 \cdot \Delta t_n(E,LO). \qquad (4)$$

This procedure yields the measurable TOF distribution for a fixed LO channel

$$\tilde{n}(t:LO) = \int d\tau \cdot T(t,\tau:LO) \cdot n(\tau:LO). \qquad (5)$$

The relativistic kinematic relation

$$E = E_0\cdot((1 - (\frac{L}{c\cdot t})^2)^{-1/2} - 1) \qquad (6)$$

(E_0 - neutron rest energy, c - light velocity, L - flight path) is used for energy scale calculation (cp. Fig. 2) as well as the determination of the energy distribution considering the functional determinant /dt/dE/.
The flight path L represents an effective value, i.e. the distance between the Cf sample and the average depth of neutron detection in the scintillator.

It is emphasized that the parameters of the γ-peak, i.e. centre and width, have to be determined with care, if the peak covers a few TOF channels only. We make use of a fit of the γ-peak to a Gaussian distribution considering the TOF channel width.

3. General principles of the analysis

The most important advantage of the two-dimensional (TOF,LO)-spectroscopy is the possibility to select the optimum LO range for the determination of N(E) as a function of E (or TOF).
The background can be excluded which appears outside the area of the detector response function, i.e. in the LO range above the neutron effect region (cp. Fig. 2). Further, the optimum LO bias is derivable to achieve the minimum error. In this way,

a high sensitivity of fission neutron spectroscopy is realized up to high E. In the present case of the long-time $^{252}Cf(sf)$ experiment, we deduced the optimum LO bias as a function of E as shown in Fig. 3. As a consequence of this analysis procedure, the detector efficiency $\varepsilon(E,B)$ has to be considered as a complex matrix. The TOF effect spectrum $n_B^C(t)$ for a given LO range (B,C) is deduced by summation upon the corresponding LO channels and the following subtraction of the background as discussed in paragraph 2.
If C is lower than the maximum value of the response function, the detector efficiency is given by

$$\varepsilon(E,B,C) = \varepsilon(E,B) - \varepsilon(E,C). \tag{7}$$

Finally, we calculate the energy spectrum $N_B^C(E)$ by the use of the relation

$$N_B^C(E) = \frac{/\frac{dt}{dE}/ \cdot \frac{1}{D} \cdot n_B^C(t(E)) \cdot K(E,\vec{\Omega})}{\bar{\nu} \cdot N_f \cdot \frac{\Delta\Omega}{4\cdot\pi} \cdot \varepsilon(E,B,C)} \tag{8}$$

(D - TOF channel width, N_f - number of counted fission events, i.e. STOP signal number, $\bar{\nu}$ - average number of neutrons per fission, K - complex correction function, see paragraph 4).
As a consequence of Eq. 8, the ratio $n_B^C/\varepsilon(E,B,C)$ must be constant. Checking this dependence in a wide B range we are able to verify the LO calibration.

The TOF scale is determined using calibrated delay devices or an appropriate precise pulser. The calibration of the LO coordinate is possible by the use of the measured two-dimensional neutron distribution itself if fitting the detector response function for fixed TOF channels, i.e. fixed E also, to the corresponding LO distributions calculated by a Monte Carlo (MC) code[15]. Here, one has to account for (i) real LO resolution parameter for the MC calculation, and (ii) the time resolution of the neutron spectrometer according to Eq. 1-5. In the case of the $^{252}Cf(sf)$ neutron spectrum which is known with a sufficient accuracy up to

about 10 MeV, the influence of the time resolution on the LO spectra to be analysed can be studied if (i) multiplying the scintillator response matrix R(E,LO) by the energy spectrum N(E) what yields

$$F(E,LO) = N(E) \cdot R(E,LO), \tag{9}$$

(ii) carrying out the transformation of F(E,LO) into a TOF distribution, (iii) folding of the resulting matrix by the time resolution function $T(t,\tau:LO)$ according to Eq. 1-5, and (iv) finally providing the inverse transformation into a neutron-energy-dependent distribution yielding $\tilde{F}(E,LO)$ to be compared with the original F(E,LO) considering the TOF bin width. Further, the scintillator response to monoenergetic neutrons can be measured and compared to the MC calculation. Additional measurements of γ response spectra (Compton distributions) are suitable to verify the LO calibration.

The detector efficiency is calculated by a MC code[15] yielding $\varepsilon_{MC}(E,B)$. Here, it is necessary to consider a realistic LO resolution parameter to be deduced by a fit of calculated response functions to experimental ones. The calculated efficiency matrix has to be normalized absolutely by additional appropriate measurements basing on nuclear standards, i.e. a normalization constant A has to be determined according to

$$\varepsilon(E,B) = A \cdot \varepsilon_{MC}(E,B). \tag{10}$$

A is a constant close to 1.0.

4. Data correction

A precise analysis of N(E) includes the consideration of several data corrections mentioned in paragraph 2 and 3 partly.

4.1. γ-peak correction. The two-dimensional (TOF,LO)-spectra have to be corrected for the LO dependent γ-peak position, if taking into account a rather large LO range. Basing on

a measurement without n/γ/μ-discrimination to deduce the reference position spectrum, the correction is carried out by a LO-channel-dependent TOF spectrum shift. However, the corrections are very small or can be neglected if restricting to high-energy neutron spectroscopy.

4.2. Transmission correction. Fission neutrons penetrate several materials between source and scintillator (fission chamber gas and wall, air, neutron detector window, scintillator wall). The corresponding transmission corrections are calculated on the base of averaged total neutron cross sections for each TOF channel. Their dependence on E is rather small in the high-energy range.

4.3. TOF-channel-dependent background due to non-correlated STOP signals. We refer to the paper of Böttger et al.[10] and consider this correction analytically. However, if dealing with moderate fission rates and analysing the high-energy range of a fission neutron spectrum, this correction was found to be neglegible.

4.4. Influence of scattered neutrons on N(E). We estimated the correction due to scattered neutrons. It is also neglegible at neutron energies above 4 MeV. This result is in agreement with an analysis of experimental (TOF,LO)-spectra (cp. Fig. 2).

4.5. Correction for time resolution. We avoid a direct spectrum unfolding because of the rare statistics at high E. An iterative method is used. The deduced non-corrected energy spectrum N(E) (cp. Eq. 8) has to be fitted to a Maxwellian distribution

$$N_M(E) = \frac{2}{\sqrt{\pi}\, T_M^{3/2}} \cdot E^{1/2} \cdot \exp(-E/T_M). \qquad (11)$$

This Maxwellian is transformed into a TOF distribution considering the detector efficiency. After folding of the resulting distribution by the time resolution function according to Eq. 1-5 with an effective resolution parameter for the chosen

LO interval, the inverse transformation is carried out yielding a zero-order correction function. This procedure is repeatet, until the folded N(E) reproduces the original spectrum within a given uncertainty. It is possible to carry out this correction for different energy segments. The described procedure is also used to deduce optimum measurement parameters in experiment conception. This concerns the flight path especially.

4.6. Bin-width correction. The gradient of a fission neutron spectrum depends on E strongly at high E especially. According to the kinematic relation (Eq. 6), the energy bin width becomes rather high. We deduce the corresponding correction function in a similar way as described in paragraph 4.5., i.e. analysis of the fitted Maxwellian spectrum. In general, an iterative treatment is not necessary, because the corrections are comparatively small.

4.7. Fragment detection efficiency. The measurable $^{252}Cf(sf)$ neutron spectrum is influenced by the anisotropic fragment detection caused by absorption in the sample plane[10,11,16] due to the deposit thickness and backing roughness. We assume an angular distribution of detected fragments given by

$$W(\beta) = (1/4\cdot\pi) \cdot (1-\exp(-\cos^2\beta/(2 \cdot s^2))) \qquad (12)$$

where the parameter s depends on the fragment efficiency ε_{FF} according to the relation

$$s = (2/\pi)^{1/2} \cdot (1- \varepsilon_{FF}). \qquad (13)$$

β is the polar angle with regard to the sample plane normal. Using the Legendre-polynominal representation of the double-differential emission probability $N(E,\Theta)$ of fission neutrons (Θ - neutron emission angle with regard to the fission axis in the laboratory frame), i.e.

$$N(E,\Theta) = \sum_i C_i(E)\, P_i(\cos\Theta), \qquad (14)$$

we obtain the measurable neutron energy distribution by numerical solution of

$$G(E,\beta) = \sum_i C_i(E)\cdot P_i(\cos\beta) \int_{-1}^{1} W(\Theta)\cdot P_i(\cos\Theta)\cdot d(\cos\Theta). \qquad (15)$$

As discribed in Ref. 3, $N(E,\Theta)$ is calculated in the framework of a complex cascade-evaporation model of fission neutron emission introducing a 10 % scission neutron component. ε_{FF} has to be determined by appropriate measurements of $G(E,\beta)$ (cp. Ref. 10,11,17).

Corrections for dead-time losses are neglegible in the case of high-energy fission neutron spectroscopy if adjusting a comparatively high electronic threshold for neutron timing. Commonly, the event rate to be recorded amounts to about (1-10) s^{-1}. Dead-time losses in the fragment detector electronics, which are determined by the fast discriminator, don't involve a renormalization, because N_f (Eq. 8) is taken to be the number of STOP signals whose counting is possible without losses.

5. Error evaluation

Obviously, the main error of fission-neutron spectroscopy at very high energies is the statistical one. In the case of rare statistics, one has to consider adequate statistical methods (see for instance Ref. 18) to deduce this error kind for a given TOF channel. The statistical error of the effect spectrum $n_B^C(t(E))$ entering Eq. 8 consists of two parts, i.e. the statistical errors of both the deduced total TOF distribution for the chosen LO range and the background.

The estimation of the detector efficiency error is a subject of a separate consideration and depends on the experimental method applied for its measurement. As described in paragraph 3, we renormalize the efficiency matrix $\varepsilon(E,B)$, which is calculated by the use of a MC code, on the base of experimental informations.

However, the experimental determination of the detector efficiency don't cover the whole energy range to be considered in analysis. Therefore, the use of the renormalized MC data implies an interpolation or extrapolation. In the present case, this concerns the energy range above 15 MeV especially.
Here, the efficiency error should be estimated considering the errors of the cross sections used in the calculation. It is emphasized that the calculated efficiency curves for a NE 213 scintillator are not strongly influenced by the less accurate neutron data for carbon (compared to the hydrogen data) at sufficiently high bias values as selected in the analysis of the high-energy spectrum end. In this case, light signals from α-particles and C recoil nuclei are suppressed. Consequently, the use of the renormalized efficiency data should be justified at high energies also.

An additional error in detector efficiency arises from the LO calibration. Considering the rough approximation

$$\varepsilon(E,B) \approx \varepsilon_0(1 - B/E) \tag{16}$$

(ε_0 is a constant), we deduce

$$\left(\frac{\Delta N}{N}\right)_{\varepsilon} = \left/ \frac{\Delta\varepsilon}{\varepsilon} \right/ \approx \Delta B/(E-B). \tag{17}$$

The error of the energy scale calibration can be transformed into the corresponding partial error $(\Delta N/N)_{ES}$ of the analysed spectrum. Taking into account the fitted Maxwellian distribution (cp. Eq. 11), one obtains

$$\left(\frac{\Delta N}{N}\right)_{ES} = \left/ \frac{1}{2} - \frac{E}{T} \right/ \cdot \left/\frac{\Delta E}{E}\right/,$$

$$\left/\frac{\Delta E}{E}\right/ \approx 2 \left/\frac{\Delta t}{t}\right/ \text{ (cp. Eq. 6).} \tag{18}$$

The errors of the data corrections are determined by the uncertainties of the main input data like time resolution,

Maxwellian temperature, TOF channel width etc. (cp. paragraph 4). Using adequately changed parameters, the correction procedures are repeated to deduce the correction error. In the case of the transmission correction, the error can be deduced from the correction formulae directly taking into account the uncertainties of both the total cross sections and the area densities.

Finally, the total error of the analysed energy spectrum is given by the uncorrelated superposition of the partial errors marked by i

$$\left(\frac{\Delta N}{N}\right)_{tot} = \left[\sum_i \left(\frac{N}{N}\right)_i^2\right]^{1/2} \qquad (19)$$

6. Results

We summarize the results of the reanalysed $^{252}Cf(sf)$ neutron spectrum measurement described in Ref. 6,7. The following synoptical table includes the main data characterizing the experimental set-up, the measurement run, and the analysis parameters.

Cf source	:	34 000 fissions per s at the beginning of the measurement, Tantalum backing (0.125 mm thick), 5 mm source diameter
Fragment detection (STOP signal)	:	fast ionization chamber[19] (1.5 at methane, 3 mm electrode distance) - preamplifier - fast amplifier - zero-cross-over timing - cable delay
Neutron detector position	:	perpendicular to the sample plane (ß = 0 deg)
Neutron detection (START signal)	:	organic scintillator NE 213 (5"x5") - fast photomultiplier XP 2041 - constant-fraction trigger
TAC range	:	200 ns
TOF bin width	:	(2.372 ± 0.007) ns

Background suppression	:	electronic charge-comparison method[13] (n/γ/μ-discrimination), heavy shielding
Flight path	:	4.500 m
Collimator	:	polyethylene, graphite liner, Pb, Fe
Running time	:	1218.5 hours subdivided in single runs, intermediate checks of thresholds, n/γ/μ-discrimination, and response signal
Average time resolution	:	(2.074 ± 0.118) ns (FWHM) with regard to γ-peak
Fragment detection efficiency	:	(0.858 ± 0.010), deduced from a 0deg/90deg-measurement of the neutron spectrum (angle with regard to sample plane normal)
Typical error of the bias energy	:	120 keV (proton energy equivalent)
γ-peak position uncertainty	:	0.10 ns

Fig. 3 shows the deduced optimum LO bias as a function of neutron energy. In general, B increases as E increases. As described in Ref. 6, the detector efficiency data calculated by means of the MC code have been checked by a separate ^{252}Cf(sf) neutron spectrum measurement at energies between 4 and 10 MeV and comparatively high bias values considering all essential data corrections (cp. paragraph 4). Fig. 4 represents the experimental efficiency data deduced by accepting the NBS evaluated spectrum[8] as the reference distribution. The agreement between experimental results and the MC calculation is rather good. The efficiency curves are reproduced in the bias region especially due to the realistic consideration of resolution effects.

Finally, we have used the spectrum in the energy range from 5 to 6 MeV (minimum experimental error in the present case) to check the efficiency data absolutely. The experimental and the calculated efficiency data were found to be in agreement within the statistical errors. Therefore, the renormalization according to Eq. 10 was neglected.

The deduced corrections as well as their uncertainties are summarized in Table 1 for the energy range (9-20) MeV. Fig. 5 represents the influence of those corrections which are strongly energy-dependent (correction for time resolution, TOF bin width, and fragment detector efficiency). Evidently, the most important partial correction is that one for time resolution. The transmission correction (cp. paragraph 4.1) is weakly energy-dependent (total (7.9 - 8.6) % above 9 MeV). The final spectrum was fitted to a Maxwellian distribution (Eq. 11) for the energy range (9-20) MeV. The deduced T_M amounts to (1.374 $\pm$ 0.020) MeV. Here the total error ΔT_M is given.

As shown in Fig. 6, the experimental data are close to the NBS evaluated spectrum at energies between 11 and 20 MeV. This conclusion was already pointed out in Ref. 6,7. In the energy range (9-11) MeV, the experimental spectrum deviates from the NBS spectrum (about -10 % departure).

The spectrum calculated in the framework of the cascade evaporation model[4] reproduces the slope of experimental data rather good but underestimates the measured data slightly. The calculation in the framework of the Madland-Nix model[20] (cp. Ref. 4 also) yields a stronger decreasing spectrum (Fig. 7).
Further, the experimental spectrum is compared with other data[9-11] which are represented as averaged values in MeV steps in Fig. 7. It is emphasized that the experimental spectra of other groups turn aside to higher values of D, i.e. the percentage departure from a Maxwellian distribution with T_M = 1.42 MeV, at the end of the measured spectrum range in each case (see Fig. 7). It seems to be a consequence of systematic influences.

The experimental errors are listed in Table 2. Above 15 MeV neutron energy, the statistical error is predominant.

The spectrum deduced above 20 MeV indicates the existence of a hard fission-neutron emission component (see Fig. 8).
In this energy range, the data corrections are neglegible excepting the transmission coefficient due to the hardness

of the spectrum. The highest-energy data are listed in Table 3. The integral yield of neutrons in the energy range (21.5 - 26.7) MeV amounts to (6.0 ± 3.4) 10^{-6} (error with 90 % confidence level). This is a surprising high value which cannot be understood in the framework of an evaporation model. We discussed the high-energy component of fission neutrons as a consequence of non-equilibrium emission in Ref. 7. It is emphasized that the stated neutron yield of highest-energy neutrons doesn't depend on the chosen bias energy. We have analysed the spectrum tail for the LO ranges (9-18) MeV and (18-30) MeV (proton energy equivalent) and obtained results which were equal within the statistical error.

Summary

Applying the (TOF,LO)-spectroscopy as well as an efficient background suppression method, fission neutron spectra are measurable up to very high emission energies. The described analysis procedure involves the selection of the optimum LO bias as a function of neutron energy. In this way, minimum errors can be obtained. Further, the analysis includes several data corrections as discussed in paragraph 4.
The time resolution has to be considered with care. This concerns the dependence on neutron energy especially (Eq. 1). A sufficiently high flight path is required to avoid too high corrections for time resolution.
Concerning the high-energy range, the spectrum corrections for fragment detector efficiency are comparatively small or can be neglected, if the neutron detector is located perpendicular to the sample plane.

Compared to the description in Ref. 6, the analysis was refined. This concerns the more exact LO calibration (see paragraph 3), the careful consideration of time resolution (Eq. 1) including the determination of the γ-peak parameter, and the more precise analysis of the neutron detector efficiency measurement.

The final data have been fitted to a Maxwellian distribution for the energy range (9-20) MeV yielding T_M = (1.374 ± 0.020) MeV. This result agrees rather good with the data of Ref. 10.
We point out that the fitted Maxwellian reproduces the measured spectrum in the high-energy range (below 20 MeV) only.
The spectrum slope is strongly changed above 20 MeV. For further conclusions, we refer to previous papers[3,7].

The support of Dr. D. Hermsdorf concerning the MC calculations and the stimulating discussions with Dr. D. Schmidt are greatefully acknowledged.

References

1) M.V. Blinov, Proc. IAEA Cons. Meet. on Neutron Source Properties, Debrecen, Hungary, 1980, INDC(NDS)-114/GT (1980)

2) Proc. IAEA Cons. Meet. on the U-235 Fast-Neutron Fission Cross-Section and the Cf-252 Fission-Neutron Spectrum, Smolenice, Czechoslovakia, 1983, INDC(NDS)-146/L (1983)

3) H. Märten et al., ibid., p. 199

4) H. Märten and D. Seeliger, J. Phys. G: Nucl. Phys. 10 (1984) 349

5) H. Märten et al., Proc. Europhysics Topical Conf. on Neutron Induced Reactions, Smolenice, Czechoslovakia, 1982, Physics and Applications 10 (1982) 287

6) H. Märten et al., INDC(GDR)-17/L (1982)

7) H. Märten et al., Proc. Int. Conf. on Nucl. Data for Sci. and Techn., Antwerp, 1982, ed. by K.H. Böckhoff, D. Reichel Publ. Comp. Eindhoven (1983) 488

8) J. Grundl and C. Eisenhauer, Natl. Bur. Stds. Publ., NBS-493 (1977)

9) M.V. Blinov et al., loc. cit. (2), p. 161

10) R. Böttger et al., loc. cit. (7), p. 484

11) W.P. Pönitz and T. Tamura, loc. cit. (7), p. 465 and loc. cit. (2), p. 175

12) S. Hayakawa, Phys. of Cosmic Rays (in russian), Moscow, 1973

13) H.-G. Ortlepp, Proc. Xth Int. Symp. on Nucl. Electronics, Dresden, 1980

14) H. Klein et al., Nucl. Instr. Meth. 193 (1982) 635

15) N.R. Stanton, COO-1545-92 (1971) and D. Hermsdorf, ZfK-315 (1977) 192

16) A. Chalupka et al., loc. cit. (2), p. 187

17) H. Märten, D. Neumann, and D. Seeliger, Proc. XIII. Int. Conf. on Nucl. Phys., Gaussig, 1983, in print

18) G. Wagner and R. Lang, Statistische Auswertung von Meß- und Prüfergebnissen, Hrsg. Deutsche Gesellschaft für Qualität e.V., Berlin und Frankfurt am Main, 1973

19) M. Adel-Fawzy et al., Kernenergie 24 (1981) 107

20) D.G. Madland and J.R. Nix, Nucl. Sci. Eng. 81 (1982) 213

Table 1

Summary of selected spectrum corrections K and their percentage errors P for neutron energies below 20 MeV. The spectrum N0(E) is already corrected for transmission. D denotes the spectrum departure from a Maxwellian distribution with T_M = 1.42 MeV (Eq. 11). The meaning of the indexes: EF - fragment detection efficiency (paragraph 4.7), FT - spectrum unfolding due to time resolution (paragraph 4.5), BW - bin width correction (paragraph 4.6).

E/MeV	$N_0(E)/MeV^{-1}$	K_{EF}/%	P_{EF}/%	K_{FT}/%	P_{FT}/%	K_{BW}/%	P_{BW}/%	$N(E)/MeV^{-1}$	D/%
8.889	.3318E-02	0.4	20	- 1.6	3.7	-0.1	70	.3275E-02	-13.8
9.292	.2455E-02	0.4	20	- 1.9	3.8	-0.1	60	.2416E-02	-17.4
9.722	.1778E-02	0.3	20	- 2.2	3.8	-0.1	55	.1742E-02	-21.2
10.184	.1325E-02	0.3	20	- 2.5	3.9	-0.2	50	.1293E-02	-20.9
10.679	.9486E-03	0.3	20	- 3.0	3.9	-0.2	47	.9211E-03	-22.0
11.211	.6887E-03	0.3	20	- 3.6	4.0	-0.3	45	.6639E-03	-20.2
11.785	.4809E-03	0.2	20	- 4.1	4.1	-0.3	42	.4607E-03	-19.1
12.404	.2969E-03	0.2	20	- 4.8	4.2	-0.4	39	.2821E-03	-25.3
13.073	.1850E-03	0.2	20	- 5.7	4.3	-0.5	37	.1739E-03	-28.2
13.799	.1213E-03	0.2	20	- 6.7	4.4	-0.6	36	.1127E-03	-24.4
14.587	.6821E-04	0.1	20	- 8.1	4.5	-0.8	35	.6220E-04	-29.4
15.445	.3648E-04	0.1	20	- 9.5	4.6	-1.0	34	.3269E-04	-34.0
16.382	.2264E-04	0.1	20	-11.5	4.8	-1.2	33	.1979E-04	-24.9
17.408	.1322E-04	0.1	20	-13.8	5.0	-1.5	32	.1121E-04	-15.0
18.534	.5552E-05	0.1	20	-16.7	5.2	-1.9	31	.4525E-05	-24.2
19.774	.1437E-05	0.0	20	-20.3	5.4	-2.4	30	.1111E-05	-55.4

Table 2

Summary of considered partial errors (16) of the $^{252}Cf(sf)$ neutron spectrum measurement for neutron energies below 20 MeV. The meanings of the indexes: ST - statistical error, BW - bin width correction, ES - energy scale, FT - unfolding correction due to time resolution, TR - transmission correction, BI - light output bias, ε - neutron detector efficiency (cp. paragraph 5).

E/MeV	$(\frac{\Delta N}{N})_{ST}$/%	$(\frac{\Delta N}{N})_{BW}$/%	$(\frac{\Delta N}{N})_{ES}$/%	$(\frac{\Delta N}{N})_{FT}$/%	$(\frac{\Delta N}{N})_{TR}$/%	$(\frac{\Delta N}{N})_{BI}$/%	$(\frac{\Delta N}{N})_{\varepsilon}$ /%	$(\frac{\Delta N}{N})_{tot}$/%
8.889	1.7	0.1	0.5	0.1	0.1	3.0	5.0	6.1
9.292	1.9	0.1	0.5	0.1	0.1	2.9	5.1	6.2
9.722	2.2	0.1	0.5	0.1	0.1	2.8	5.2	6.3
10.184	2.5	0.1	0.5	0.1	0.1	2.6	5.4	6.5
10.679	3.0	0.1	0.5	0.2	0.1	2.5	5.5	6.8
11.211	3.4	0.1	0.5	0.2	0.1	2.4	5.7	7.1
11.785	3.9	0.1	0.5	0.2	0.1	2.1	5.9	7.4
12.404	5.0	0.2	0.5	0.3	0.1	2.0	6.1	8.2
13.073	6.2	0.2	0.6	0.3	0.1	1.8	6.3	9.0
13.799	7.6	0.2	0.6	0.4	0.1	1.7	6.5	10.2
14.587	8.9	0.3	0.6	0.5	0.1	1.6	6.8	11.3
15.445	12.7	0.3	0.6	0.6	0.1	1.5	7.1	14.7
16.382	15.6	0.4	0.6	0.7	0.1	1.3	7.4	17.3
17.408	21	0.5	0.6	0.9	0.1	1.2	7.7	22.4
18.534	36	0.6	0.6	1.1	0.1	1.1	8.0	37
19.774	88	0.7	0.7	1.4	0.1	1.0	8.4	88

Table 3

Experimental data on the high-energy end of the ^{252}Cf(sf) neutron spectrum (E above 20 MeV)

E/MeV	$N(E)/MeV^{-1}$	$\Delta N(E)/MeV^{-1}$ x)
20.8	.203E-05	.154E-05
22.3	.110E-05	.080E-05
24.0	.159E-05	.100E-05
25.8	.131E-05	.120E-05
27.9	.130E-05	.120E-05
30.2	.410E-06	.940E-06

x) 75 % confidence level

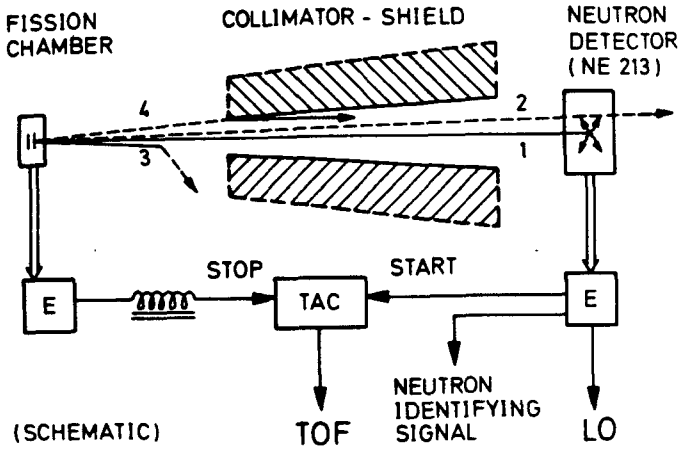

Fig. 1

Schematic representation of the experimental set-up. Fission neutrons (1,2) are detected within the fixed solid angle $\Delta\Omega$ with an efficiency $\varepsilon(E,B)$. The measured spectrum is disturbed by neutron absorption (3) and scattering (4) at surrounding materials including air (E - standard nuclear electronic devices, TAC - time-to-amplitude-converter).

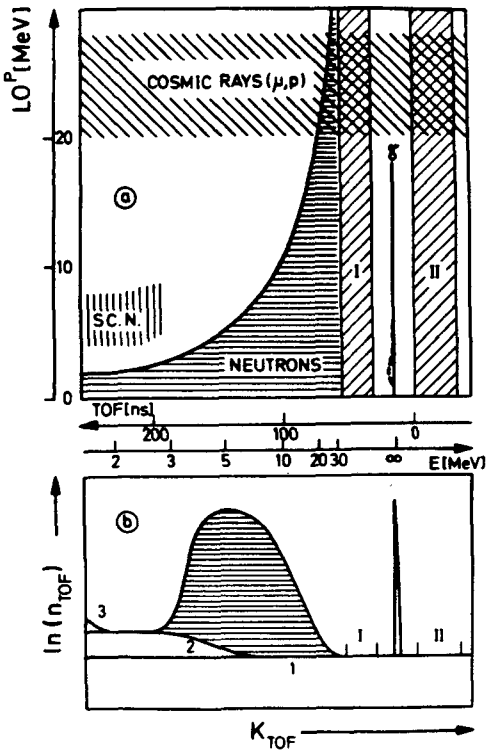

Fig. 2a

Schematic illustration of the (TOF,LO)-spectrum (SC. N. - scattered neutrons, I,II - regions for the determination of the random background)

Fig. 2b

Typical TOF spectrum (schematic) for a selected LO bias (1 - random background, 2 - channel-dependent background due to non-correlated STOP-signals, 3 - background caused by scattered neutrons, cp. Fig. 1).

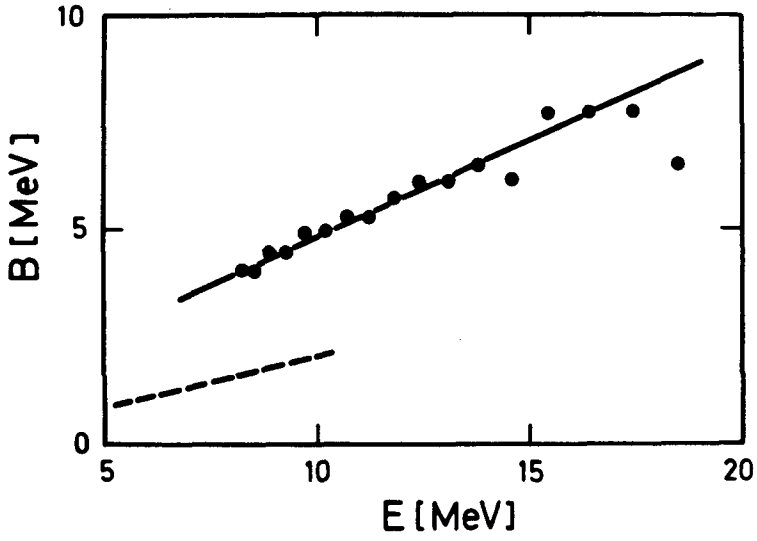

Fig. 3

Optimum LO bias B (with regard to proton energy) as a function of neutron energy. The points represent the deduced data. The continous line is shown to guide the eyes. The dashed line indicates achievable conditions. In the present case, the dynamic range of the particle discrimination unit was chosen in such a manner that cosmic myons are suppressed efficiently.

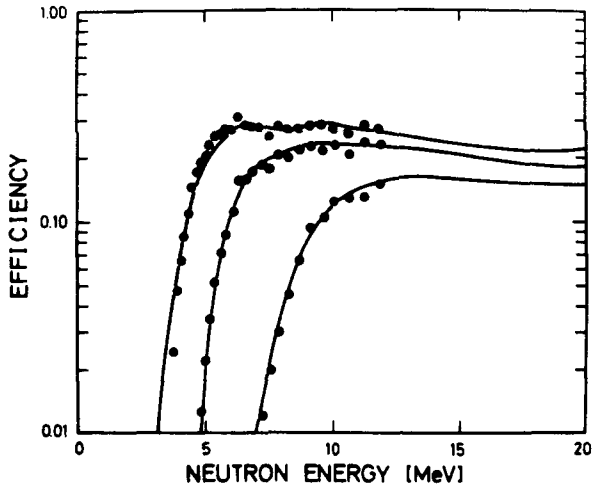

Fig. 4

Experimental data on detector efficiency deduced from a ^{252}Cf(sf) neutron spectrum measurement applying Eq. 8 in comparison with the MC calculation. The data are shown at relatively high bias values (3.76 MeV, 5.01 MeV, and 7.5 MeV with regard to proton energy).

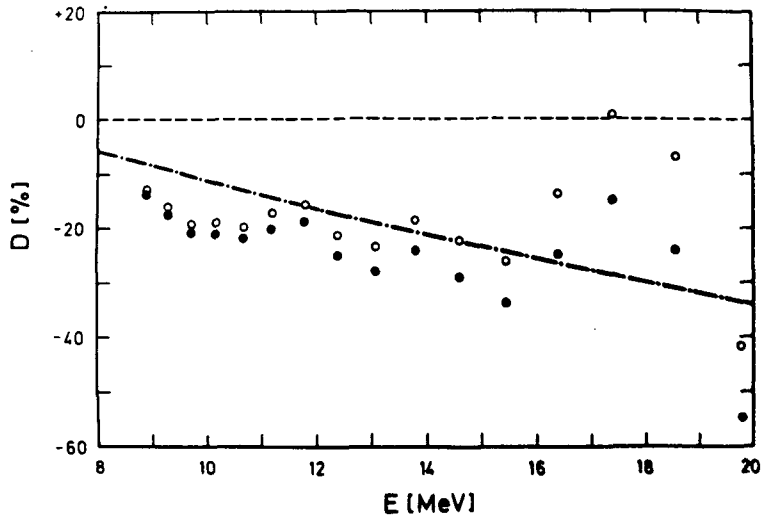

Fig. 5

Non-corrected (o) and corrected (•) data on the $^{252}Cf(sf)$ neutron spectrum[6,7] represented as percentage departures D from a Maxwellian distribution with T_M = 1.42 MeV. In this figure, data corrections for time resolution, TOF bin width, and fragment detection efficiency are considered (cp. Table 1). The dashed-dotted curve represents the NBS evaluated spectrum[8].

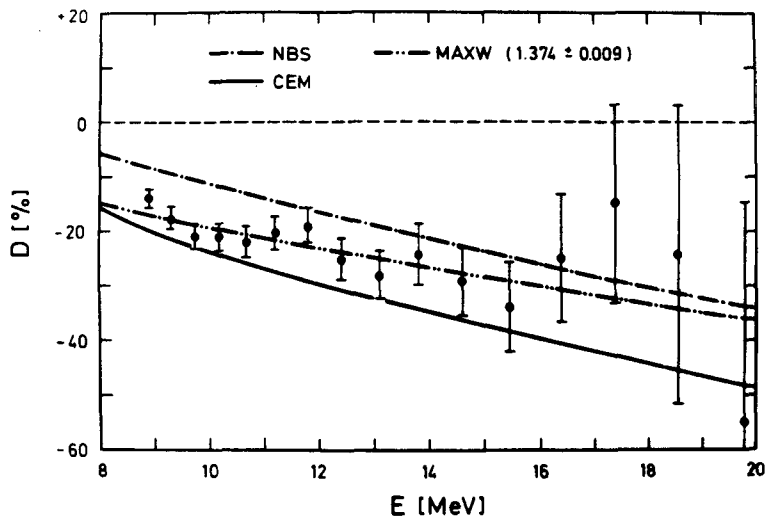

Fig. 6

Percentage departures D of the experimental data from a Maxwellian distribution with T_M = 1.42 MeV in comparison with the NBS evaluated spectrum, a calculated spectrum deduced in the framework of a complex cascade evaporation model, and a fitted Maxwellian distribution with T_M = (1.374 ± 0.009) MeV. Here, the statistical error of T_M is presented.

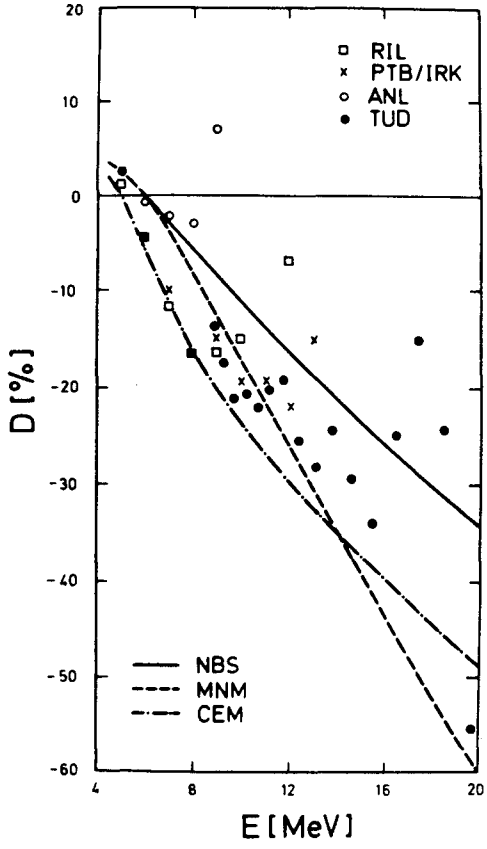

Fig. 7

Comparison of our experimental data (TUD) both with the results of other groups (RIL[9]), PTB/IRK[10]), ANL[11])) and theoretical spectrum curves (MNM - Madland-Nix model version[4]), CEM - cascade evaporation model[4]), NBS - evaluated spectrum[8])). D denotes the percentage departure from a Maxwellian with T_M = 1.42 MeV.

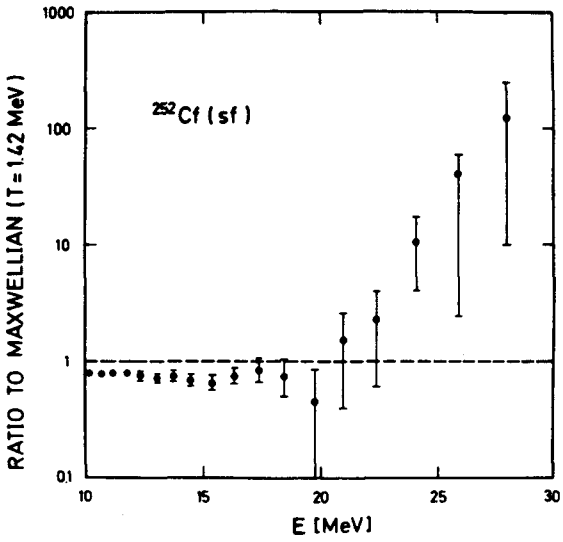

Fig. 8

Experimental data on the high-energy end of the ^{252}Cf(sf) neutron spectrum.